

CLOSURE PHASE SIGNATURES OF PLANET TRANSIT EVENTS

GERARD T. VAN BELLE¹

European Southern Observatory, Garching, Germany 85748
gerard.van.belle@eso.org

Accepted for publication in PASP

ABSTRACT

Planet transit events present as attractive targets for the ultra-high-resolution capabilities afforded by optical interferometers. Herein is presented an evaluation of the possibility of detection of such events through measurement of high-precision closure phases with the MIRC instrument on the CHARA Array. Recovery of the transit position angle upon the sky appears readily achievable with the existing capabilities of the instrument, along with characterization of other system parameters, such as stellar radius, planet radius, and other parameters of the transit event. This technique is the only one presently available that can provide a transiting planet's orbital plane position angle, and can directly determine the planet's radius independent of any outside observations, appearing able to improve substantially upon other determinations of that radius. Additional directly observed parameters - also not dependent upon transit photometry or spectroscopy - include impact parameter, transit ingress time, transit velocity and stellar radius.

Subject headings: techniques: interferometric, techniques: high angular resolution, stars: planetary systems, stars: individual: HD189733

1. INTRODUCTION

Recent discoveries of stars exhibiting the telltale signs of planet transits has begun to add a new layer of understanding to the rapidly developing field of exoplanetology. While the technique of radial velocity detection has produced the greatest yield to date of planet detections (Butler et al. 2006), the detected transit events have served to define the specific nature of those planets, including parameters such as density, atmospheric composition, and aspects of system dynamics (Burrows et al. 2006).

Advances in the state of the art in astronomical optical interferometry can be directed at these recent transit discoveries and also contribute to filling in the pieces of the exoplanet puzzle. Specifically, measurements of interferometric closure phase during a planet transit event can determine the inclination and orientation of the planetary orbit upon the sky, in addition to refining the angular diameter measurements of both the planet and the star. Just as the Rossiter-McLaughlin effect (Rossiter 1924; McLaughlin 1924) in radial velocity measurements can contribute to our knowledge of transiting planet system parameters (Winn et al. 2006), transit event closure phases can further the physical description of these systems through direct detection of the transit. Interferometric phase in general is a powerful tool that is beginning to be exploited to its fullest potential in astronomy (Monnier 2007).

Planet transit closure phase observations described herein are the only presently available technique that provide a measurement of the transiting planet's orbital plane orientation upon the sky. These closure phase observations also uniquely determine the other observables of the system - impact parameter, transit velocity, stellar radius, planet radius, transit ingress time - without the need for supporting observations such as transit pho-

tometry. For example, the previous direct determination of HD189733b's diameter (Baines et al. 2007) measured that parameter through a combination of interferometric measurements and transit photometry; this technique is independent of such outside measurements.

We will begin with a review of instrument capabilities in §2, an examination of known extrasolar planet candidates in §3, a 'quick-and-dirty' partial analytic solution of the problem in §4, a more thorough discussion of closure phase leading to a numeric model and analysis of planet transits in §5, and finally a full Monte Carlo simulation to recover synthetic transits in §6.

2. INSTRUMENT CAPABILITIES

The Georgia State University Center for High Angular Resolution Astronomy (CHARA) Array is a six-element optical interferometer located atop Mount Wilson in southern California. The CHARA Array consists of six 1-m telescopes laid out on a 'Y' array, two telescopes per arm, with a baselines of > 300 meters on the 3 longest baselines. Initial science operations and a facility description can be found in McAlister et al. (2005) and ten Brummelaar et al. (2005).

Commissioning on-sky tests have recently begun at the CHARA Array with the Michigan Infrared Combiner (MIRC), a high-precision multi-telescope beam combiner (Monnier et al. 2006a). MIRC's capability to combine 4 or 6 telescopes simultaneously and provide 3 to 10 closure phase measurements on sources represents a major step forward in capability for the facility. Moreover, initial MIRC tests are indicating a remarkable ability to measure closure phases with precision unprecedented in the field of optical interferometry, at a level of $\sigma_\phi \sim 0.03^\circ$ Monnier et al. (2006a); the first science demonstrated by this capability includes direct imaging the surface of the rapidly rotating star Altair (Monnier et al. 2007). Other instruments, such as the VLTI AMBER instrument (Rantakyro et al. 2006), also provide the capability to make closure phase measurements, although initial in-

¹ For preprints, please email gerard.van.belle@eso.org.

dications are that the closure phase precision of AMBER is not quite as capable as MIRC, with $\sigma_\Phi \sim$ few degrees (Weigelt et al. 2007).

3. POTENTIAL PLANET TRANSIT TARGETS

The obvious candidate for observations of a planet transit event is HD189733 (Bakos et al. 2006; Bouchy et al. 2005). With an angular size of $376 \pm 31 \mu\text{s}$ (Baines et al. 2007), it is the planet-transit hosting star with the largest angular size discovered to date. The discovery paper of Bouchy et al. (2005) cites the following system parameters: (a) a planet-star radius ratio of 0.172 ± 0.003 , (b) an orbital inclination of $i = 85.79 \pm 0.24$, (c) an orbital radius of 0.0313 ± 0.0004 AU, and (d) a transit duration of roughly 1.7 hours. The geometry of the transit is depicted in Figure 1. The best known values for the host star and planet are found in Tables 1 and 2, respectively.

The next best candidate known at the time of this draft is GJ 436 (Butler et al. 2004; Gillon et al. 2007), with roughly the same anticipated angular size as HD189733. HD149026 (Sato et al. 2005), HD17156 (Fischer et al. 2007; Barbieri et al. 2007), and HD209458 (Henry et al. 1999; Charbonneau et al. 2000) are also worth considering, although their stellar angular diameters of 170–250 μs are significantly less favorable for detection when considering the currently available capabilities of CHARA-MIRC.

4. PARTIAL ANALYTIC SOLUTION FOR TRANSIT INTERFEROMETRIC VISIBILITY

The complex interferometric visibility of a binary star can be written as:

$$V_{\text{binary}} = e^{-2\pi i(u\alpha_1 + v\beta_1)} \frac{V_A + rV_B e^{-2\pi i(u\Delta\alpha + v\Delta\beta)}}{1 + r} \quad (1)$$

where r is the brightness ratio (Herbison-Evans et al. 1971). V_A and V_B are the visibility functions associated with a uniform disk, $V = 2J_1(x)/(x)$, where $x = \theta_{UD}\pi B/\lambda$, θ_{UD} is the uniform disk angular diameter, B is the projected baseline, and λ is the wavelength of operation. Dropping the absolute phase term and rewriting this in terms of relative separation vector $\Delta\mathbf{s}$ and baseline vector \mathbf{B} :

$$V_{\text{binary}} = \frac{V_A + rV_B e^{-2\pi i\mathbf{B}\cdot\Delta\mathbf{s}/\lambda}}{1 + r} \quad (2)$$

Determining visibilities for the specific case of a planet transit can be adopted from this formalization with the following caveats:

- The ‘brightness ratio’ r is the negative value of the squared planet-to-star diameter ratio.
- Equation 2 assumes that both the planet and stellar disks are indeed uniform disks, since r is constant. Specifically, limb darkening of the star is ignored.
- Equation 2 is valid only for the portion of the transit event when the planet is fully in front of the star, when r is again constant. The ingress and egress portions of the transit event are not properly represented by this equation.

This solution is useful in characterizing the order-of-magnitude effects for observation planning; however, given the above caveats, it is insufficient for proper evaluation of actual data.

5. TRANSIT CLOSURE PHASE AND VISIBILITY DEVIATIONS

In its simplest realization, an optical interferometer measures the Fourier components of an image upon the sky. The location of the image’s components in the Fourier transformed $\{u, v\}$ plane are dictated by the baseline between the telescopes in the interferometer projected towards the source of interest, and the wavelength of operation. As seen in §4, at least a partial analytic solution can be predicted from the parameters of the experiment. In practice, only the visibility amplitude (typically just referred to as the *visibility*) can be measured, while atmospheric turbulence corrupts the direct measurement of visibility phase.

However, interferometers using three or more telescopes can produce a measurement of the *closure phase*, a phase quantity that remains uncorrupted by telescope-specific phase errors (Jennison 1958; Monnier 2000). The closure phase Φ is the sum of visibility phases around a closed loop of baselines. For three telescopes i, j, k , this is easily deduced from the observed visibilities:

$$\Phi_{ijk} = \arg(V_{ij}) + \arg(V_{jk}) + \arg(V_{ki}) \quad (3)$$

Each pair of telescopes produces a source visibility and phase, where the phase is associated with the source’s intrinsic phase ϕ , phase errors $\theta_1 - \theta_2$ associated with the telescope pair, and noise. Typically due to atmospheric corruption, for a pair of telescopes, phase information is useless. However, for a three telescope array $\{l, m, n\}$, combination of the three measured phase pairs ($\psi_{lm} = \phi_{lm} + (\theta_l - \theta_m), \dots$) results in cancelation of the phase error terms θ leaving only the sum of the three source phases intrinsic to the object - the closure phase, $\Phi_{lmn} = \phi_{lm} + \phi_{mn} + \phi_{nl}$.

Use of the closure phase effectively cancels many of the corrupting effects of the atmosphere and the instrument, and is a highly sensitive probe for interferometric image construction on the smallest spatial scales. Significantly more complete discussions of the topic of closure phase may be found in Pearson & Readhead (1984) and Monnier (2007). Closure phases have been used to explore disk asymmetries in YSOs (Monnier et al. 2006b) and are very sensitive to asymmetries in images, which will prove quite useful in the application discussed here.

For a star with a planet blocking out part of its disk during a transit event, the degree of asymmetry is extreme - significantly much more so than a star with a starspot on its surface: the spot temperature is merely some slight fraction of the rest of the photosphere and is still emitting radiation at a fairly significant level. At the near-infrared wavelengths being considered here, a transiting planet emits extremely little radiation with regards to the area of the stellar photosphere it is blocking off from our line of sight.

For the full envelope of expected visibility amplitudes and closure phases for a *gedanken* experiment covering the interferometer response during a planet transit event, the analytic solution of §4 is insufficient, in that it breaks down during the transit ingress and egress. As a means to

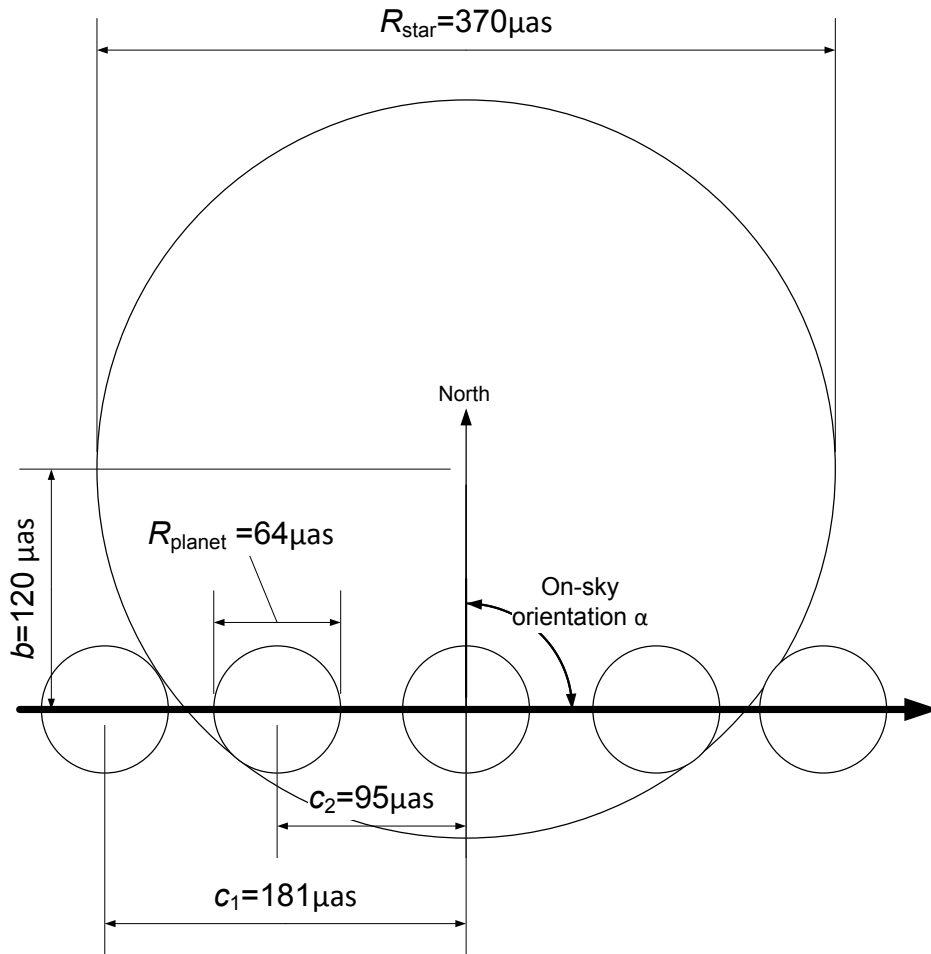


FIG. 1.— On-sky geometry for a model representative of HD189733, based on data found in Bouchy et al. (2005) and Baines et al. (2007), as discussed in §3. In particular, the planet radius of $R_{\text{planet}} = 64\mu\text{as}$ and impact parameter $b = 120\mu\text{as}$ are derived from the stellar radius, the planet-star radius ratio, and orbital inclination. The values of $c_1 = 181$ and $c_2 = 95\mu\text{as}$ mark the distance of the beginning and end of the ingress event from the transit meridian. The on-sky orientation of the transit chord is, at present, unknown.

TABLE 1
SUMMARY OF PARENT STAR PARAMETERS FOR HD189733.

Parameter	Value	Units	Reference
UD Angular Size	366 ± 31	μas	Baines et al. (2007)
Limb darkening coefficient	1.9	%	Tango & Davis (2002)
LD Angular Size	372 ± 31	μas	Baines et al. (2007)
Bolometric Flux	28.28 ± 0.49	$10^{-9} \text{ erg cm}^{-2} \text{ s}^{-1}$	Baines et al. (2007)
Parallax	51.94 ± 0.87	mas	Perryman et al. (1997)
Effective Temperature	4980 ± 200	K	
Linear radius	0.779 ± 0.066	R_{\odot}	Baines et al. (2007)
Mass	0.82 ± 0.05	M_{\odot}	Bouchy et al. (2005)
Luminosity	0.305 ± 0.008	L_{\odot}	
log g	4.607 ± 0.043	$[\text{cm s}^{-2}]$	

explore that full envelope, a numeric analysis can be performed to compute directly the expected visibility components.

For the specific case of HD189733, such an experiment may easily be executed, leading to an expectation of the changes in observed visibility amplitudes and closure phases during the planet transit event. For the *gedanken* experiment, three baselines

were postulated, with coordinates (in meters) of $\{125.35, 305.94\}$, $\{-300.42, -89.62\}$, $\{175.07, -216.32\}$ (with zero vertical separation), which correspond roughly to the CHARA E1S1, W1E1, and S1W1 baselines, respectively.

From the system parameters for HD189733 as cited by Bouchy et al. (2005), a model of the transit event was constructed with a stellar radius of $185\mu\text{as}$, a planet ra-

TABLE 2
SUMMARY OF EXOPLANET PARAMETERS FOR HD189733.

Parameter	Value	Units	Reference
Radius ratio	0.172 ± 0.003		Bouchy et al. 2005
Angular diameter	64.0 ± 5.4	μas	
Linear Radius	1.19 ± 0.10	R_{jup}	Baines et al. (2007)
Density	0.91 ± 0.23	g cm^{-3}	Baines et al. (2007)

dius of $32\mu\text{as}$, and a transit chord that was offset from the center of the stellar disk by $121\mu\text{as}$. The rate of the transit was not considered in this section, in this simple inspection of the effects upon the interferometer visibility signals, although in §6 variables for that aspect of the event will be introduced. The top panels of Figure 2 shows the this transit event for three different orientations upon the sky, $\alpha = 0^\circ, 45^\circ, 90^\circ$.

For each of the three orientations, the visibility for each of the three baselines, along with the closure phase, was computed. This computation was performed in the following manner: An appropriately limb darkened model star was created numerically on a 1024×1024 grid with a diameter corresponding to the HD189733 parent star. As introduced by Milne (1921) and discussed in the context of stellar interferometry by Hanbury Brown et al. (1974), the conventional linear representation of limb darkening across the disk of a star can be written as:

$$I_\lambda(\mu) = I_\lambda(1)[1 - u_\lambda(1 - \mu)] \quad (4)$$

where $\mu = \cos\gamma$, γ is the angle between the line of sight and the stellar surface normal, and $I_\lambda(1)$ is the specific intensity at the center of the disk. For HD189733 at $5000 \pm 100\text{K}$ (Baines et al. 2007), the limb darkening parameter u at $1.6\mu\text{m}$ is roughly equal to 0.35 (Claret et al. 1995); as we shall see in §6, this technique is relative insensitive to limb darkening of the planet host star. This latter fact is unsurprising given the small angular size of the star relative to our notional array; for an array with larger baselines ($B \sim 1\text{km}$), there would a greater sensitivity to this parameter.

A fully darkened spot corresponding to the radius of the transiting planet was then created on the image for a given location along that transit, and the Fourier components were computed. Rather than bear the full computational load of Fourier transforming the entire image upon the sky, the approach of Aufdenberg et al. (2006) is followed, and only the specific components corresponding to the 3 baselines in question were computed, resulting in a much lighter computational load without a sacrifice in precision.

This process was then repeated for various points along the planet transit. The computed values for visibility and closure phase were compared to the nominal values for the uneclipsed parent star, and those deviations are plotted in the middle and lower panel of Figure 2. This approach to computing the visibility amplitudes and closure phases can be seen as being superior to the analytic solution in §4, since it takes into account stellar limb darkening, and is valid through the transit event, including ingress and egress.

As seen in Figure 2, during the transit event, the visibility deviates from from the nominal unocculted star

case, but by only a marginal amount - on the order of $\pm 0.01\%$. Such a measurement is beyond the capabilities of any existing interferometer by two orders of magnitude. However, the closure phase excursion is $\pm 0.2^\circ$. As detailed in Monnier et al. (2006a), closure phase measurements at this level of precision appear possible: initial tests of the CHARA-MIRC system showed closure phase formal error at the $\sigma_\Phi \sim 0.03^\circ$ level over the course of 3 hours. Shorter integration times indicated a correspondingly higher level of scatter, but the magnitude of this error gives a starting point from which to evaluate the possibility for observation of a planet transit event using closure phases.

6. RECOVERY OF TRANSIT PARAMETERS FROM CLOSURE PHASE MEASUREMENTS

Having demonstrated in §5 in at least a qualitative way that closure phase excursions result from a planet transit event, it is useful to further demonstrate that an event can be reconstructed from an ensemble of closure phase measurements taken during a transit. Free parameters of the fit are the primary descriptors of the image upon the sky:

- The stellar radius r_{star} .
- The planet to star radius ratio R .
- The orbit orientation upon the sky α , defined as the angular orientation of the chord of the transit event across the disk of the star in right ascension and declination, as measured from north to east on the sky.
- The ‘impact parameter’ b , defined as the distance between the chord of the transit event across the disk of the star, and the center of the stellar disk.
- The ‘zero time’ JD_0 of the transit event, defined here as the time of closest approach of the planet disk to the center of the stellar disk.
- The velocity v of the planet disk across the disk of the star.

Fixed input parameters of the fit are:

- The $i = 1 \dots N$ closure phases Φ_i and their associated errors $\sigma_{\Phi,i}$. For this exercise, it will be assumed that these are the single closure phases associated with the non-diurnally evolved CHARA baselines associated with the S1, S2, E1, and W1 stations. In practice, CHARA-MIRC is operated with either four or six simultaneous baselines, which in the latter case can potentially provide even more closure phases than being modelled here; this, in conjunction with baseline diurnal evolution, would serve to further constrain the transit event parameters.
- The closure phase errors $\sigma_{\Phi,i}$. These errors were assumed to have a normal distribution, and for the various synthetic data sets created below, assumed to be of a magnitude ranging from $\overline{\sigma_{\Phi,i}} = 0.005^\circ, 0.010^\circ, 0.020^\circ, 0.050^\circ, 0.100^\circ$. The FWHM of the $\sigma_{\Phi,i}$ distribution was set at one-quarter of

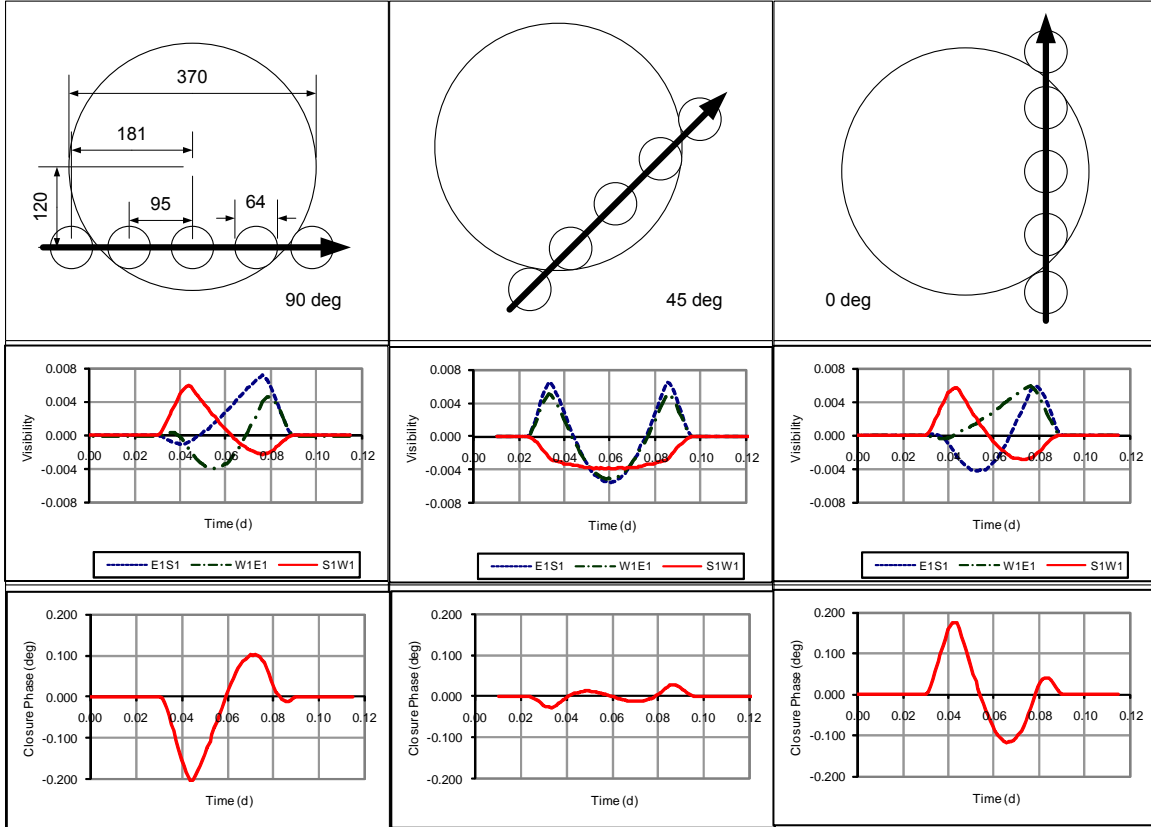


FIG. 2.— Excursions in visibility amplitude and closure phase data for HD 189733 as observed by CHARA for 3 different orientations, as discussed in §6. The top row is the image on the sky, the middle row is the visibility amplitude excursions for each of the 3 CHARA baselines discussed herein, and the bottom row is the closure phase difference during the transit event.

the average error value. Individual closure phases Φ_i were randomized by an error of the scope of σ_{Φ_i} (but independent thereof).

- The operational wavelength λ_i of each observation of the closure phases. A single wavelength of $1.6 \mu\text{m}$ will be assumed here for the synthetic data sets. In practice, the MIRC instrument spectrally disperses the starlight and multiple closure phases per observation are available as a result.
- The time t_i of observation of each closure phase. For our synthetic data sets, we will postulate that sets of closure phases are taken sequentially at intervals of 0.001 of a Julian Day (roughly 85 seconds set-to-set), for a total duration of 0.124 days (about 3 hours), which spans the duration of the transit event, plus about 40 minutes before and after the transit event. This resulted in $N = 124$ data points per observation set.
- The $\{u, v\}$ coordinates of observing baselines for each closure phase, For an actual observation, the baselines would need to be properly projected onto the sky incorporating diurnal motion.
- The limb darkening of the star.

The stellar limb darkening is also potentially fittable free parameter; however, for the marginal resolution case of

CHARA observing HD189733, a model value is sufficient for the fitting.

For simplicity of this investigation, diurnal motion will be ignored and the $\{u, v\}$ coordinates of the observing baselines will be constant. In practice, this motion will need to be accounted for but will actually provide addition constraints upon the image reconstruction, much in the same way that baseline evolution can serve to assist in constraining the parametrization of binary star orbits (Boden et al. 1999).

To create synthetic ‘observation sets’ for testing our fitting and parameter recovery routines, the free parameters $\{r_{star}, R, b, JD_0, v\}$ discussed at the beginning of this section were set to the values seen in our HD189733-like system in Figure 1 (with $JD_0 = -6000$ sec, $R = 0.17$, $b = 121.0 \mu\text{as}$, $r_{star} = 185 \mu\text{as}$, and $v = 0.07000 \mu\text{as}/\text{sec}$), and data sets were generated within the context of the fixed input parameters discussed above. For those data sets, the position angle α of the planet transit across the stellar disk was also set to the values 28° , 115° , and 170° , to test the sensitivity of the parameter recovery on that particular parameter as well.

Thus, to test ‘goodness of fit’ for a given set of six randomized free parameters $\{r_{star}, R, \alpha, b, JD_0, v\}$, a model transit event sequence was generated, projected upon the sky, and resultant image sequence Fourier transformed for comparison to each of the observed Φ_i data points, and a χ^2/DOF calculated. A multi-dimensional optimization code was then utilized to loop

about this goodness of fit routine and derive the best $\{r_{star}, R, \alpha, b, JD_0, v\}$ solution from any given starting point, a process that took typically 500 iterations (Press et al. 1992). An exhaustive search of the transit event parameter space was used to explore the χ^2/DOF space, using a two-fold approach. First, a grid of reasonable $\{r_{star}, R, \alpha, b, JD_0, v\}$ starting values was explored to see if the original $\{r_{star}, R, \alpha, b, JD_0, v\}$ parameters could be recovered, with α varying over its full range of $\{0^\circ, 360^\circ\}$, and the other parameters being explored over a range of $\pm 50\%$ of their ‘true’ values. These latter ranges were expected to encompass the reasonable starting points for an actual investigation, based upon constraints that may be available from discovery photometry or spectroscopy. Each range was gridded with a density of 5 to 10 points per variable. Second, a large number of iterations ($N \sim 1000$) were also run for each synthetic data set starting from fully randomized $\{r_{star}, R, \alpha, b, JD_0, v\}$ starting values, also with the purpose of recovering the original $\{r_{star}, R, \alpha, b, JD_0, v\}$ parameters that described the generating values of the synthetic data set. The resulting χ^2 manifold appeared to be smoothly varying, as the recovery of the original parameters appeared to occur without local minima obstructing the recovery of the global minima. Once the best solution was established for a given data set, $1 - \sigma$ errors were established about the χ^2 minimum through exploration of appropriate $\Delta\chi^2$ intervals. The results for each of the three transit position angles, with the five different levels of closure phase error, are seen in Table 3.

7. DISCUSSION AND CONCLUSION

Examination of Table 3 illustrates that, even with a crude level of closure phase error ($\overline{\sigma_\phi} \sim 0.1^\circ$), the position angle of the transit event is readily recovered to within a few degrees, and markedly better with modest improvements in closure phase error. Since closure phase is, in essence, an observable that quantifies the degree of asymmetry in an image upon the sky, we expect that this technique should work well even for grazing transit events. These events would be limited presumably by the shorter duration of the occultation event (and thus fewer closure phase data points to fit), and also by a lesser stellar surface area occulted by the planet’s disk, resulting in a smaller closure phase signal, but the basic promise of the approach holds true. The sensitivity of this approach to limb darkening - mentioned, but largely dismissed in §6 - is only slight, due to the largely axisymmetric nature of limb darkening.

Of particular interest is the fact that, in the best conceivable case for each apparent transit position angle, the planet radius appears to be recoverable to the level of roughly one part in 30-40, which appears to best the previous interferometric measure of the planetary diameter (Baines et al. 2007) by a factor of 2.5. Additionally, the technique establishes that diameter in a way that is independent of the transit photometry - the Baines et al. (2007) investigation relied upon transit photometry for a value of the planet-star radius, R .

There is further the possibility that conducting such an observation in a wavelength-dependent sense could probe molecular opacity effects of the the planetary atmosphere though sensing apparent radius dependencies. For example, the recent detection of methane as an constituent of HD189733b’s atmosphere (Swain et al. 2008) provides a tantalizing goal for this technique; in principle, a sufficiently precise measurement of this nature, using narrow channels inside of the H -band (say, comparing 0.05 μm -wide channels centered at 1.5, 1.66, and 1.73 μ , respectively) could confirm this detection by detecting the wavelength dependence of the planetary radius. However, this appears to require levels of closure phase precision beyond even the best cases considered here - an examination of the absorption depth data of Swain et al. (2008) indicates such a detection to require radius measurement precision at the 0.2 – 1.1% level.

These simulations use *only* the time-tagged closure phase data from a single transit event; supporting photometric and radial velocity signatures of the transit (and interferometer visibility measures), or multiple transits, have the potential to significantly improve the quality of the $\{r_{star}, R, \alpha, b, JD_0\}$ fit parameters. Investigators wishing to mesh such data sets will of course have to pay particular attention to uniform time-tagging. It does seem possible, however, that data sets of such richness will be able to probe other system parameters: possible moons of the transiting planet, and the presence of other stellar planetary companions due to variations in the transit timing and impact parameter.

This approach is the **only** currently available technique that provide any value for the transit event orientation angle, α ; it is also an independent check on parameters such as stellar radius or planet-star radius ratio that is derived from other techniques, such as spectroscopy or photometric timing. Use of results from such interferometric observations could be highly useful for planning observations of TPF-I, Darwin, and other instruments that have a position-angle dependent response. For example, the extreme adaptive optics systems that are envisioned carrying out planet searches and/or characterizations through ‘dark hole’ techniques (Serabyn et al. 2007; Oppenheimer et al. 2008) could have their search times reduced through *a priori* knowledge of the planet’s orbital plane position angle.

Special thanks to Theo ten Brummelaar, John Monnier, Mark Swain, and Ming Zhao for particularly helpful feedback during the development of this manuscript, which also benefited greatly from the input of an anonymous referee. The CHARA Array is funded by the National Science Foundation through grant AST 94-14449, the W. M. Keck Foundation, the David and Lucile Packard Foundation, and by Georgia State University. This research has made use of the SIMBAD literature database, operated at CDS, Strasbourg, France, the FUTDI database at AMNH, and of NASA’s Astrophysics Data System.

REFERENCES

Aufdenberg, J. P., et al. 2006, ApJ, 645, 664

Baines, E. K., van Belle, G. T., ten Brummelaar, T. A., McAlister, H. A., Swain, M., Turner, N. H., Sturmman, L., & Sturmman, J. 2007, ApJ, 661, L195

- Bakos, G. Á., et al. 2006, *ApJ*, 650, 1160
- Barbieri, M., et al. 2007, *A&A*, 476, L13
- Boden, A. F., et al. 1999, *ApJ*, 515, 356
- Bouchy, F., et al. 2005, *A&A*, 444, L15
- Butler, R. P., Vogt, S. S., Marcy, G. W., Fischer, D. A., Wright, J. T., Henry, G. W., Laughlin, G., & Lissauer, J. J. 2004, *ApJ*, 617, 580
- Butler, R. P., et al. 2006, *ApJ*, 646, 505
- Burrows, A., Sudarsky, D., & Hubeny, I. 2006, *ApJ*, 650, 1140
- Charbonneau, D., Brown, T. M., Latham, D. W., & Mayor, M. 2000, *ApJ*, 529, L45
- Claret, A., Diaz-Cordoves, J., & Gimenez, A. 1995, *A&AS*, 114, 247
- Cody, A. M., & Sasselov, D. D. 2002, *ApJ*, 569, 451
- Fischer, D. A., et al. 2007, *ApJ*, 669, 1336
- Gillon, M., et al. 2007, *A&A*, 472, L13
- Hanbury Brown, R., Davis, J., Lake, R. J. W., & Thompson, R. J. 1974, *MNRAS*, 167, 475
- Henry, G. W., Marcy, G., Butler, R. P., & Vogt, S. S. 1999, *IAU Circ.*, 7307, 1
- Herbison-Evans, D., Hanbury Brown, R., Davis, J., & Allen, L. R. 1971, *MNRAS*, 151, 161
- Jennison, R. C. 1958, *MNRAS*, 118, 276
- McLaughlin, D. B. 1924, *ApJ*, 60, 22
- Milne, E. A. 1921, *MNRAS*, 81, 361
- McAlister, H. A., et al. 2005, *ApJ*, 628, 439
- Monnier, J. D. 2000, *Principles of Long Baseline Stellar Interferometry*, 203
- Monnier, J. D., et al. 2006a, *Proc. SPIE*, 6268
- Monnier, J. D., et al. 2006b, *ApJ*, 647, 444
- Monnier, J. D., et al. 2007, *Science*, 317, 342
- Monnier, J. D. 2007, *New Astronomy Review*, 51, 604
- Oppenheimer, B. R., et al. 2008, *ArXiv e-prints*, 803, arXiv:0803.3629
- Pearson, T. J., & Readhead, A. C. S. 1984, *ARA&A*, 22, 97
- Press, W.H., Teukolsky, S.A., Vetterling, W.T., Flannery, B.P., 1992, *Numerical Recipes in C*, Port Chester, Cambridge University Press
- Rantakyö, F. T., et al. 2006, *Proc. SPIE*, 6268
- Rossiter, R. A. 1924, *ApJ*, 60, 15
- Sato, B., et al. 2005, *ApJ*, 633, 465
- Serabyn, E., Wallace, K., Troy, M., Mennesson, B., Haguenaer, P., Gappinger, R., & Burruss, R. 2007, *ApJ*, 658, 1386
- Swain, M. R., Vasisht, G., & Tinetti, G. 2008, *ArXiv e-prints*, 802, arXiv:0802.1030
- Tango, W. J., & Davis, J. 2002, *MNRAS*, 333, 642
- ten Brummelaar, T. A., et al. 2005, *ApJ*, 628, 453
- Weigelt, G., Driebe, T., Hofmann, K.-H., Kraus, S., Petrov, R., & Schertl, D. 2007, *New Astronomy Review*, 51, 724
- Winn, J. N., et al. 2006, *ApJ*, 653, L69

TABLE 3

RESULTS FROM FITTING TRANSIT EVENT PARAMETERS TO THREE SYNTHETIC TRANSIT CLOSURE PHASE DATA SETS AS DISCUSSED IN §6. ORIGINAL VALUES WERE $JD_0 = -6000$ SEC, $R = 0.17$, $b = 121.0\mu\text{AS}$, $r_{\text{star}} = 185\mu\text{AS}$, AND $v = 0.07000\mu\text{AS}/\text{SEC}$.

Input Position Angle (α) [deg]	$\overline{\sigma_\Phi}$ [deg]	Time Zero (JD_0) [sec]	Ratio Planet-Star Radius (R)	Impact Parameter (b) [μas]	Recovered Position Angle (α) [deg]	Star Radius (r_{star}) [μas]	Planet Speed (v) [$\mu\text{as}/\text{sec}$]	Planet Radius (r_{planet}) [μas]	Planet Radius Fractional Error
28	0.005	-5981 ± 20	0.1709 ± 0.0061	119.9 ± 2.6	27.87 ± 0.26	185.2 ± 1.7	0.07000 ± 0.00047	31.7 ± 1.17	27.1
28	0.010	-6075 ± 38	0.1701 ± 0.0074	123.2 ± 2.2	28.25 ± 0.42	185.5 ± 2.7	0.06900 ± 0.00092	31.6 ± 1.45	21.8
28	0.020	-5969 ± 53	0.1687 ± 0.0115	114.1 ± 5.9	27.02 ± 0.82	183.2 ± 4.3	0.06900 ± 0.00180	30.9 ± 2.23	13.9
28	0.050	-6268 ± 97	0.1717 ± 0.0126	137.1 ± 6.3	27.67 ± 1.40	189.1 ± 7.3	0.07100 ± 0.00352	32.5 ± 2.69	12.1
28	0.100	-5917 ± 183	0.1748 ± 0.0352	124.5 ± 12.2	25.98 ± 2.98	183.3 ± 18.2	0.07000 ± 0.00640	32.0 ± 7.19	4.5
115	0.005	-5955 ± 28	0.1719 ± 0.0047	123.1 ± 1.2	115.52 ± 0.37	184.3 ± 1.9	0.07000 ± 0.00097	31.7 ± 0.93	34.2
115	0.010	-6020 ± 21	0.1690 ± 0.0038	120.3 ± 1.8	114.95 ± 0.42	185.3 ± 1.5	0.07000 ± 0.00095	31.3 ± 0.75	41.8
115	0.020	-6011 ± 41	0.1700 ± 0.0075	120.1 ± 3.4	114.84 ± 0.85	184.4 ± 2.4	0.06900 ± 0.00143	31.3 ± 1.44	21.7
115	0.050	-5874 ± 77	0.1708 ± 0.0121	123.9 ± 5.6	115.37 ± 1.70	180.3 ± 5.7	0.06800 ± 0.00321	30.8 ± 2.39	12.9
115	0.100	-5957 ± 155	0.1742 ± 0.0178	136.2 ± 12.8	115.34 ± 2.64	184.7 ± 8.1	0.06900 ± 0.00507	32.2 ± 3.58	9.0
170	0.005	-6005 ± 12	0.1694 ± 0.0051	121.4 ± 1.6	170.13 ± 0.31	185.6 ± 1.8	0.07100 ± 0.00121	31.4 ± 0.99	31.6
170	0.010	-6001 ± 17	0.1703 ± 0.0053	121.8 ± 2.1	170.05 ± 0.44	183.8 ± 1.5	0.06900 ± 0.00065	31.3 ± 1.01	31.1
170	0.020	-5920 ± 36	0.1698 ± 0.0076	120.2 ± 4.5	168.51 ± 0.67	181.0 ± 2.9	0.06800 ± 0.00182	30.7 ± 1.46	21.0
170	0.050	-5943 ± 65	0.1715 ± 0.0193	122.0 ± 6.6	168.04 ± 1.31	186.7 ± 5.3	0.06900 ± 0.00281	32.0 ± 3.72	8.6
170	0.100	-5893 ± 236	0.1696 ± 0.0275	123.7 ± 13.6	168.12 ± 4.87	178.1 ± 13.3	0.06400 ± 0.00756	30.2 ± 5.39	5.6